Long mean free paths of room-temperature THz acoustic phonons in a high thermal conductivity material

Ting-Han Chou, Lucas Lindsay, Alexei A. Maznev, Jateen S. Gandhi, Donna W. Stokes, Rebecca L. Forrest, Abdelhak Bensaoula, Keith A. Nelson, and Chi-Kuang Sun

Phys. Rev. B **100**, 094302 — Published 4 September 2019

DOI: 10.1103/PhysRevB.100.094302

Long mean free paths of room-temperature THz acoustic phonons in a high thermal conductivity material

Ting-Han Chou,[1] Lucas Lindsay,[2] Alexei A. Maznev,[3*] Jateen S. Gandhi,[4] Donna W. Stokes,[4] Rebecca L. Forrest,[4] Abdelhak Bensaoula,[4†] Keith A. Nelson[3] & Chi-Kuang Sun[1*]

[1]*Department of Electrical Engineering and Graduate Institute of Photonics and Optoelectronics, National Taiwan University, Taipei 10617, Taiwan*

[2]*Materials Science and Technology Division, Oak Ridge National Laboratory, Oak Ridge, Tennessee 37831, USA*

[3]*Department of Chemistry, Massachusetts Institute of Technology, Cambridge, Massachusetts 02139, USA*

[4]*Department of Physics, University of Houston, Houston, Texas 77204, USA*

[*]Author to whom correspondence should be addressed: sun@ntu.edu.tw, alexei.maznev@gmail.com

[†]Present address: Institute of Physics, Academia Sinica, Taipei 11574, Taiwan

Abstract

We report measurements of room-temperature mean free paths of long-lived THz acoustic phonons in wurtzite GaN. Longitudinal phonon wavepackets are excited and probed by femtosecond laser pulses in two InGaN-GaN multiple quantum well structures separated by a GaN layer. By measuring the temperature dependence of the phonon attenuation in the range 80–300 K we isolate the intrinsic phonon mean free path at 300 K which is found to be 5.3 and 3.5 μm at 1.06 and 1.43 THz, respectively. The measurements are found to be in a good agreement with *ab initio* calculations which show that the main channel of the acoustic phonon decay is a three-phonon scattering process involving the acoustic phonon and two high-frequency optical phonons. Our results indicate that the contribution of low-THz acoustic phonons to thermal transport in GaN is relatively smaller than in Si, thus finite size effects are expected to be less important in GaN.

I. INTRODUCTION

Semiconductors and dielectric materials with high thermal conductivity (k) are important for thermal management of microelectronic devices. In these materials, heat is primarily carried by acoustic phonons in the THz frequency range. Phonon mean free path (MFP), i.e., the average distance that a phonon travels before being scattered, is the key parameter controlling a phonon's capacity to carry heat and the material thermal conductivity [1]. The knowledge of scattering mechanisms that limit MFPs of THz acoustic phonons is crucial to understanding phonon-mediated thermal transport. While the spectrum of acoustic phonons often extends to ~10 THz, recent research has indicated that long-MFP phonons in the low-THz frequency range may make a large contribution to room temperature (RT) thermal conductivity. For example, phonons with frequencies below 2 THz have been predicted to contribute ~50% to the RT thermal conductivity of silicon [2]. The large contribution of low-THz, long-MFP phonons explains recent observations of non-diffusive thermal transport in Si and other materials at RT at micron distances [3-6]. Thus these phonons are especially important for micro- and nano-scale thermal transport applications, as in many materials they control the length scale at which the bulk k value can no longer be used to describe heat conduction [3-9].

In high quality single crystal materials, acoustic phonon lifetimes and MFPs at RT are mainly limited by anharmonic phonon-phonon scattering [7]. Within the past decade, advances in theory and computational power have made *ab initio* calculations of

phonon-phonon scattering rates tractable [10-13]; thus phonon lifetimes and MFPs can be calculated from first-principles for many materials. However, these calculations have only been tested by comparison with thermal conductivity measurements [10-13], which provide information integrated over the entire phonon spectrum. Inelastic x-ray and neutron scattering techniques have been used to determine THz phonon lifetimes from linewidths in scattering spectra for several low *k* materials [14-18]. These measurements generally did not yield good agreement with *ab initio* calculations [16-19]; indeed, these low *k* systems tend to be strongly anharmonic and/or disordered, which presents a challenge for perturbation methods employed in the calculations. The existing theory framework is expected to work much better for more harmonic high thermal conductivity materials. However, inelastic x-ray and neutron scattering techniques are incapable of dealing with long-lived phonons in high *k* materials due to their limited instrumental resolution. Picosecond ultrasonics, in which coherent phonons are excited and probed by femtosecond laser pulses, is capable of measuring phonon lifetimes and MFPs directly [20-26]. However, despite the demonstrated ability to generate coherent longitudinal acoustic (LA) phonons at frequencies above 1 THz [27,28], there are no experimental data on RT intrinsic (associated with phonon-phonon interactions) phonon lifetimes in high thermal conductivity materials above 0.47 THz [23].

Gallium nitride (GaN) is a high thermal conductivity semiconductor widely used in power electronics and solid-state lighting. Thermal transport in GaN-based devices has been

the subject of intense research efforts [29]. GaN possesses high k with a measured RT value of 230 $Wm^{-1}K^{-1}$ [30], and an even higher k value of 400 $Wm^{-1}K^{-1}$ has been predicted for isotopically pure GaN [12]. Meanwhile, InGaN/GaN multiple quantum well (MQW) structures yield excellent performance in the laser generation and detection of coherent phonons [27,31]. Measurements of phonon lifetimes in GaN both below and above 1 THz have been attempted [23-26], but only yielded lower bounds for the intrinsic phonon MFP due to extrinsic factors such as scattering by interface roughness and non-uniformity of GaN layer thickness within the measurement spot [26].

In this article, we perform optical pump-probe measurements on double InGaN/GaN MQWs to measure the intrinsic lifetimes and MFPs of >1 THz LA phonons in GaN and compare them with *ab initio* calculations. Building upon the experimental approach of Ref. [26], we performed temperature-dependent measurements to isolate the intrinsic lifetimes, added an additional pump pulse to eliminate the effect of photoexcited carriers on the measured acoustic amplitude, and systematically examined important experimental parameters that limit measurement accuracy, including laser spot position, pump power, and probe wavelength. The experimental results agree with *ab initio* calculations, indicating that 1 THz LA phonons in GaN are primarily limited by interactions between the heat-carrying acoustic phonon and two high-frequency optical phonons. In addition, we estimate the contribution of low-frequency acoustic phonons to thermal transport directly from the

measured phonon lifetimes and discuss the implications for the performance of GaN for heat dissipation on the microscale.

II. EXPERIMENT DETAILS

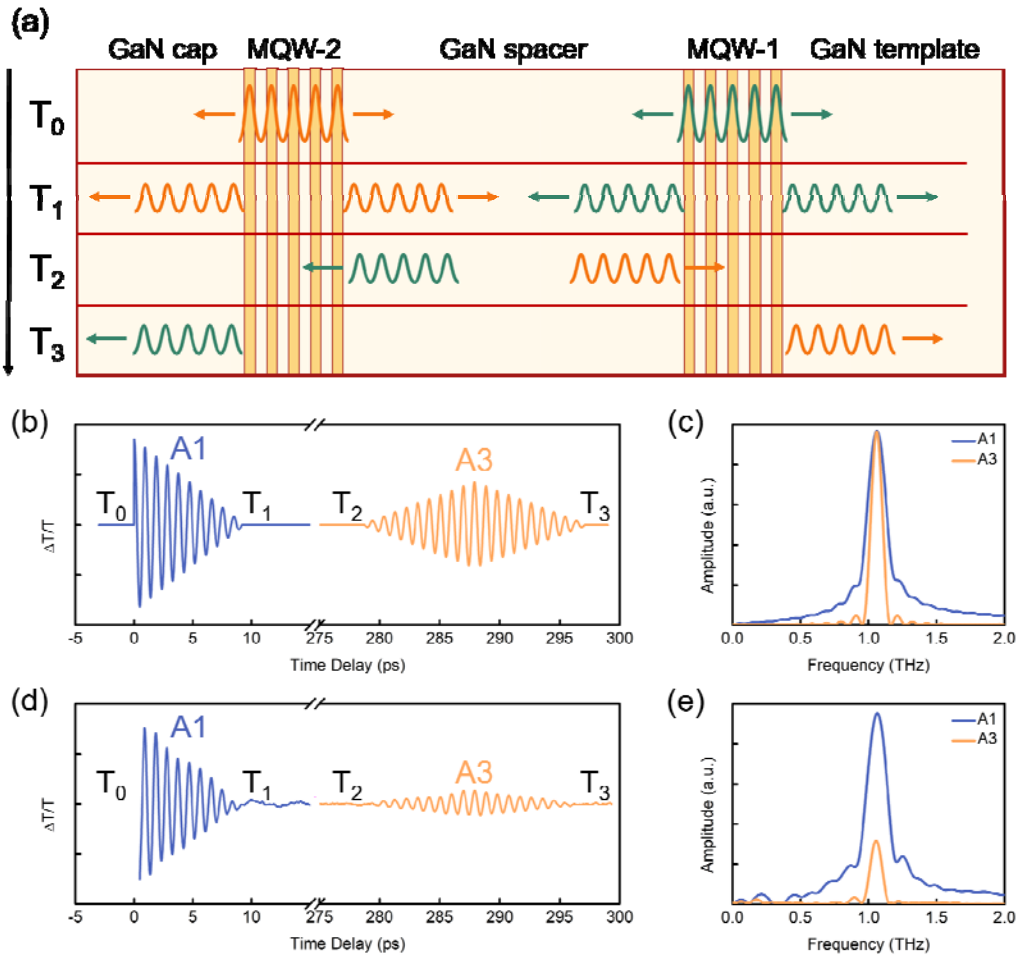

FIG. 1 (a) Schematic of the sample structure and coherent acoustic wavepackets generated and detected in two identical MQWs. Each MQW has 10 periods (only 5 periods shown here). The horizontal direction corresponds to the crystal *c* axis. At time T_0 each MQW launches two counter-propagating phonon wavepackets. At T_1 the wavepackets exit the MQWs. At T_2 two wavepackets enter the MQWs after traversing the GaN spacer. At T_3 the wavepackets have left the MQWs. (b) Simulation of the acoustic signals from sample 1 in the absence of attenuation. A1 and A3 represent the first and the third acoustic signals. (c) Fourier spectra of simulated A1 and A3. (d) Measured experiment signals of A1 and A3 from sample 1. (e) Fourier spectra of measured A1 and A3.

The sample structure contains two identical $In_{0.2}Ga_{0.8}N$/GaN MQWs separated by a GaN

spacer layer, as illustrated in Fig. 1(a). Upon femtosecond optical excitation, LA phonon wavepackets with the frequency determined by the periodicity of the MQW structures [31] were simultaneously generated, propagated through the GaN spacer layer, and simultaneously detected by the two MQWs. Both MQW-1 and MQW-2 have 10 periods with the same thickness of GaN barriers and InGaN wells. Sample 1 was designed for ~1 THz LA phonons with a InGaN/GaN MQW period of 7.5 nm and a 2.28 μm-thick GaN spacer layer, while sample 2 was designed for ~1.4 THz LA phonons with a MQW period of 5.5 nm and a 1.16 μm-thick spacer layer. The thicknesses of the GaN spacer layer and the MQW period were determined from transmission electron microscopy images (see Supplemental Material [32]).

Figure 1(b) shows the simulation results of acoustic signals measured from sample 1 in the absence of any losses. The strain-induced transmission change of the probe beam $\frac{\Delta T}{T}$ can be derived as a convolution function [33]

$$\frac{\Delta T}{T} = N \times \int_{-\infty}^{+\infty} S(z - vt)F(z)dz, \quad (1)$$

where $S(z,t)$ is strain amplitude as a function of time t and position z (c-axis in GaN), v is the acoustic velocity of phonon wavepacket in GaN, $F(z)$ is the detection sensitivity function of the MQWs, and N is the number of phonon wavepackets that overlap with the MQWs. We regard the strain amplitude as a cosine function with 1.06 THz frequency and assume that the sensitivity function is a square wave with ~40% duty ratio (where the value of 3 nm wells is 1 and 4.5 nm barriers is 0). At time T_0, InGaN/GaN MQWs absorbed an

optical pump pulse, generated free carriers, and launched two counter-propagating phonon wavepackets in opposite directions via the inverse piezoelectric effect [31]. From time T_0 to T_1, four phonon wavepackets travelled out of the MQW regions, producing the first acoustic signal (A1) with a triangular envelop. From time T_1 to T_2, phonons travelled through the GaN spacer layer and the phonon wavepackets launched from MQW-1 (MQW-2) enter the MQW-2 (MQW-1) region simultaneously. From time T_2 to T_3, two phonon wavepackets travelled through the MQW regions, producing the third acoustic signal (A3) with a diamond-shaped envelope. The full response also contained the second and the fourth acoustic signals generated by phonon wavepackets reflected from the sample surface, which did not enter our analysis. Figure 1(c) shows that the Fourier peaks of A1 and A3 were expected to have the same magnitude in the absence of attenuation. With a shorter temporal envelope, A1 possessed a broader bandwidth than A3 in the frequency domain. As shown in Fig. 1(d), in the experiment (to be discussed below) the shape of the measured A1 and A3 signals gave good agreement with the simulation. A1 was observed near zero time delay, while A3 appeared after a propagation time of 288 ps across the GaN spacer layer. The first oscillation peak in the simulated A1 was not resolvable in the experiment because it was overwhelmed by the background signal near zero time delay (see Fig. 2(a)) [25] and the amplitude of the measured A3 was significantly smaller than that of the simulated A3. Figure 1(e) shows the Fourier-transform spectra of the measured A1 and A3 signals yielding a peak

at a frequency of 1.06 THz, with A3 yielding a smaller peak magnitude than A1, indicating that the phonon wavepackets were attenuated during propagation through the GaN spacer layer. Thus, by comparing the peak magnitudes of A1 and A3 in the Fourier spectra (P1 and P3, respectively), we quantify the acoustic attenuation (P3/P1) and calculate the phonon lifetime in GaN.

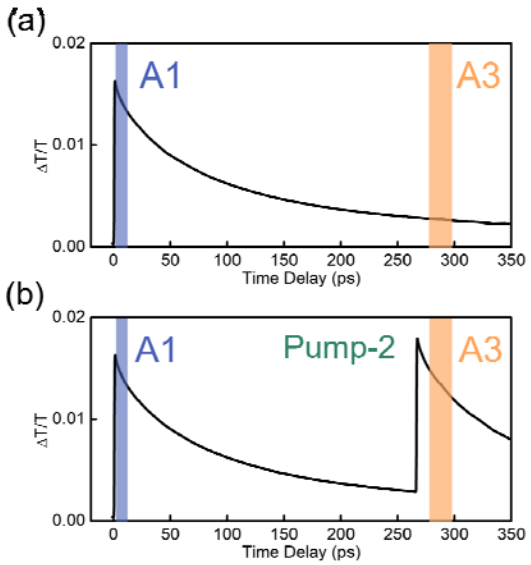

FIG. 2 Measured probe transmission changes in sample 1 (a) without and (b) with pump-2. The blue and orange regions represent the locations of A1 and A3, respectively.

The optical pump-probe experiments were carried out using a frequency-doubled Ti:sapphire laser with ~200 fs pulse duration. The pump and probe wavelengths were tuned between 390–410 nm, corresponding to photon energies above the bandgap of InGaN but below GaN. The optical fluences of pump and probe were 140 and 28 μJ/cm^2, respectively, and the laser spot diameter at the sample was ~11 μm. The sample was placed in a cryostat under vacuum for temperature-dependent measurements. Further details of the experiment setup are given in Supplemental Material [32]. Figure 2(a) shows the pump-probe trace

measured from sample 1 at RT with 404 nm probe wavelength. A sudden rise of the optical probe transmission produced by photo-excited carriers was observed near time zero and was followed by a slow decay due to carrier dynamics. Acoustic oscillations in the signal were obscured by the carrier dynamics background, but became visible after the subtraction of the slowly decaying background. For example, after subtracting the slowly decaying background in Fig. 2(a), we obtained the acoustic signals shown in Fig. 1(d). By the time the A3 signal was observed, the carrier density in the MQWs had decayed significantly. Since the photo-excited carrier density may affect the detection mechanism of coherent acoustic phonons [34], the sensitivity function may be different for A1 and A3, as we have indeed observed. Consequently, the measured optical signal change may not reflect the true acoustic attenuation. To remedy this challenge, we introduced a second pump pulse (pump-2) to recover the carrier density in MQWs. Pump-2 arrived 10-20 ps before A3; the delay was chosen to make sure that the additional acoustic signal produced by pump-2 (see Figs. 3(a), 3(b), and 3(d)) would not interfere with A3. The incident energy of pump-2 was adjusted to ensure that the signal produced by the electronic excitation, that is the carrier dynamic background signal shown in Fig. 2(b), had the same amplitude during the detection of A1 and A3, to ensure the same carrier concentration in the MQWs. With the same photo-excited carrier density in MQWs, we thus assumed that the sensitivity function was the same for A1 and A3.

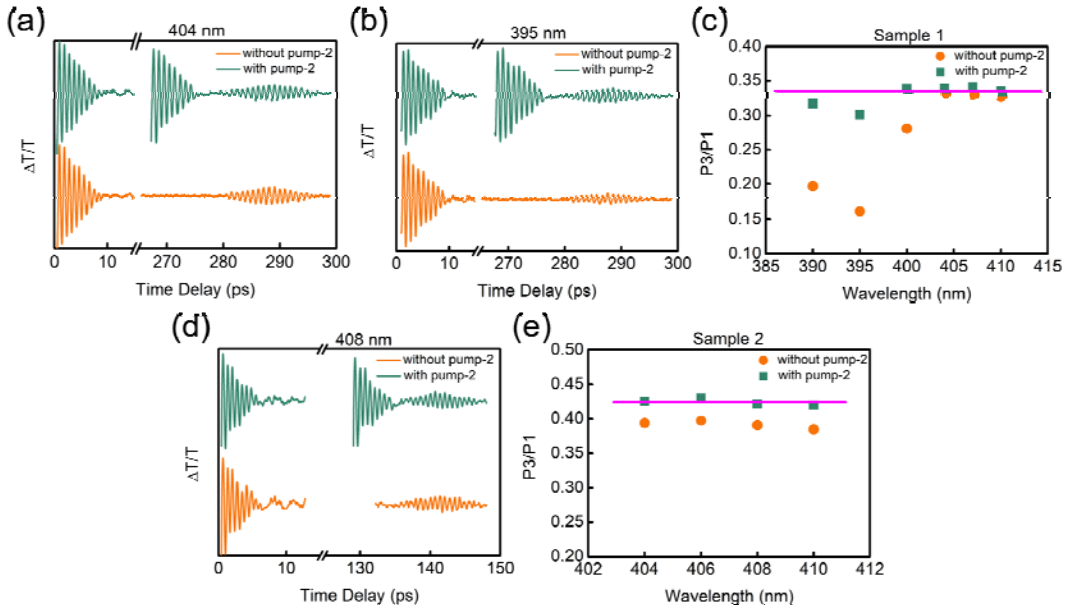

FIG. 3 (a), (b) Acoustic signals measured from sample 1 with and without the second pump (pump-2) using the probe wavelength of 404 nm and 395 nm. (c) The measured 1.06 THz phonon lifetime versus probe wavelength. (d) Acoustic signals measured from sample 2 with and without pump-2 using the probe wavelength of 408 nm. (e) The measured 1.43 THz phonon lifetime versus probe wavelength.

To test the validity of our approach, we investigated the impact of pump-2 on the phonon detection sensitivity. The photo-excited carrier density may enhance phonon detection and this effect should be probe wavelength-dependent [34]. We performed measurements with different probe wavelengths with and without pump-2. The optical fluences of pump-1, pump-2, and the probe were tuned to 140, ~140 (depending on carrier background signal), and 28 μJ/cm^2. Figures 3(a) and 3(b) shows the results of the wavelength-dependent measurements on sample 1. When the probe wavelength was tuned to 404 nm, we observed that A3 remains almost unchanged with and without pump-2. In contrast, when probe wavelength was tuned to 395 nm, we observed a large enhancement of A3 (around 288 ps) with the injection of pump-2, and the measured P3/P1 was recovered

from a false value of ~0.16 back to ~0.33. It clearly demonstrates the detection sensitivity recovery for A3 by injecting pump-2. Figure 3(c) shows that the measured P3/P1 ratios remained relatively constant at different wavelengths with the injection of pump-2. The measurements on sample 2 are shown in Figs. 3(d) and 3(e). The smaller MQW period yielded oscillated signals with a higher frequency of 1.43 THz and the thinner spacer layer yielded a shorter propagation time of 141.3 ps. When the probe wavelength was tuned from 404 to 410 nm, each measurement showed that A3 was slightly enhanced by pump-2 and the measured P3/P1 ratio was slightly increased. These results reveal that correct acoustic attenuation (P3/P1) can be obtained using proper probe wavelength for measurements on sample 1, while for measurements on sample 2, the assistance of pump-2 is always needed to avoid the effect of the reduced photo- carrier density on the sensitivity function. Therefore, in the following experiments, we used 408 nm probe wavelength with pump-2 for sample 2, while measurements on sample 1 were conducted without pump-2 at 404 nm probe wavelength.

III. RESULTS AND DISCUSSION

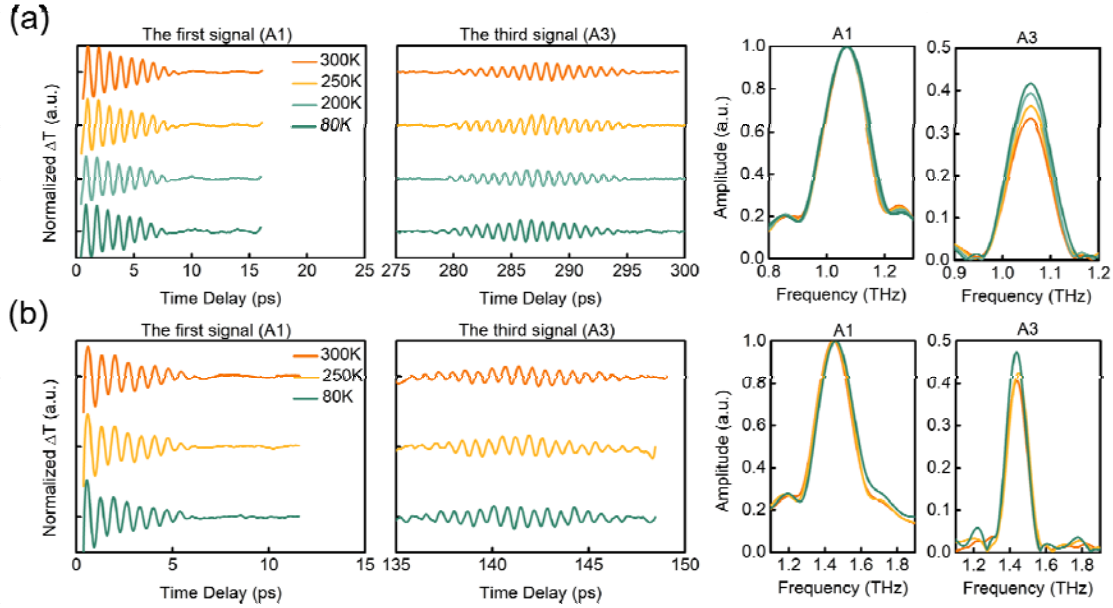

FIG. 4 (a) The normalized A1 and A3 signals (normalized by P1) and the corresponding Fourier spectra from sample 1 at 300, 250, 200, and 80 K. (b) The normalized A1 and A3 signals (normalized by P1) and the corresponding Fourier spectra from sample 2 at 300, 250, and 80 K.

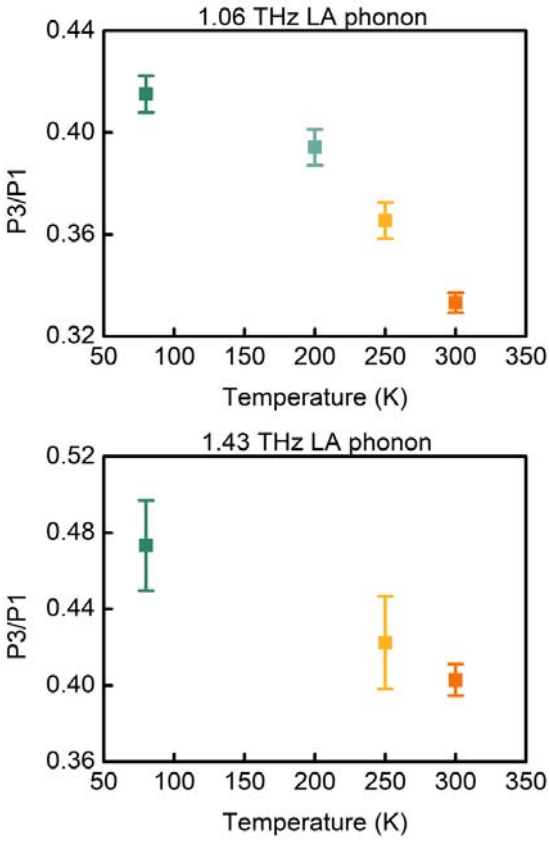

FIG.5 Acoustic attenuation (P3/P1) measured from sample 1 and sample 2 versus temperature. Each data point was obtained by analyzing 50–100 pump-probe scans. The measurements were repeated for 5–10 times (each time we averaged 10 pump-probe scans) and the error bars represented the corresponding standard deviations (see Supplemental Material [32]).

We performed temperature-dependent measurements in order to obtain the intrinsic true phonon lifetimes. The measured acoustic attenuation (P3/P1) can be expressed as

$$\frac{P_3}{P_1} = \varepsilon \cdot \exp\left[-\frac{T}{2\tau_{in}}\right] \quad (2)$$

where T is the phonon propagation time in the GaN spacer layer (T=288 ps for sample 1, while T=141.3 ps for sample 2), τ_{in} is the intrinsic phonon lifetime in GaN, and the factor ε accounts for the temperature-independent attenuation such as GaN thickness non-uniformity [26], as well as scattering by sample imperfections. Since these extrinsic factors are strongly related to quality of the sample and may vary with the laser spot position, we used a diamond pen and scratched a pattern on the sample to define a reference position and used an optical microscope to *in situ* ensure that the laser spot was at the same position (relative to the reference position) during temperature-dependent measurements.

We relied on the temperature dependence of the measured acoustic attenuation to isolate the intrinsic phonon lifetime τ_{in}. Figures 4(a) and 4(b) show the normalized A1 and A3 signals (the Fourier peak magnitude of each A1 (P1) is normalized to 1) and the corresponding frequency spectra for 1.06 and 1.43 THz LA phonons versus temperature. The Fourier peak magnitude of A3 (P3) gradually increased, which indicated that the attenuation decreased, as temperature was lowered. Figure 5 summarizes the measured acoustic

attenuations (P3/P1) for 1.06 and 1.43 THz LA phonons versus temperature. To calculate the intrinsic phonon lifetime in GaN at 300 K (the same method was also used for 250 and 200 K), we excluded the extrinsic temperature-independent attenuation by comparing the P3/P1 measured at 300 and 80 K. According to Eq. (2), the intrinsic phonon lifetime can be obtained as follows,

$$\frac{2}{T}\left[\ln\left(\frac{P_3}{P_1}\right)^{80K} - \ln\left(\frac{P_3}{P_1}\right)^{300K}\right] = \frac{1}{\tau_{in}^{300K}} - \frac{1}{\tau_{in}^{80K}} \approx \frac{1}{\tau_{in}^{300K}} \quad . \tag{3}$$

The above equation assumes that the intrinsic scattering rate at 80 K is negligible compared to that at 300 K, due to a significant decrease of the thermal phonon population at 80 K. We will see shortly that this assumption is supported by *ab initio* calculations. We obtained an intrinsic 1.06 THz LA phonon lifetime at RT of 655±62.4 ps, corresponding to a ~5.3 μm phonon MFP (the LA phonon velocities in the range 1.06–1.43 THz are equal to the low-frequency constant longitudinal acoustic velocity along the *c* axis v_L=8020 m/s [27,35]), while at 1.43 THz the measured intrinsic phonon lifetime was 438.3±147.2 ps, corresponding to a ~3.5 μm phonon MFP. Note that while we obtained the MFP values from the lifetimes, we could also calculate the MFP directly by replacing the time delay *T* in Eq. (3) by the GaN layer thickness. Thus, our method provides direct measurements of both phonon lifetime and MFP.

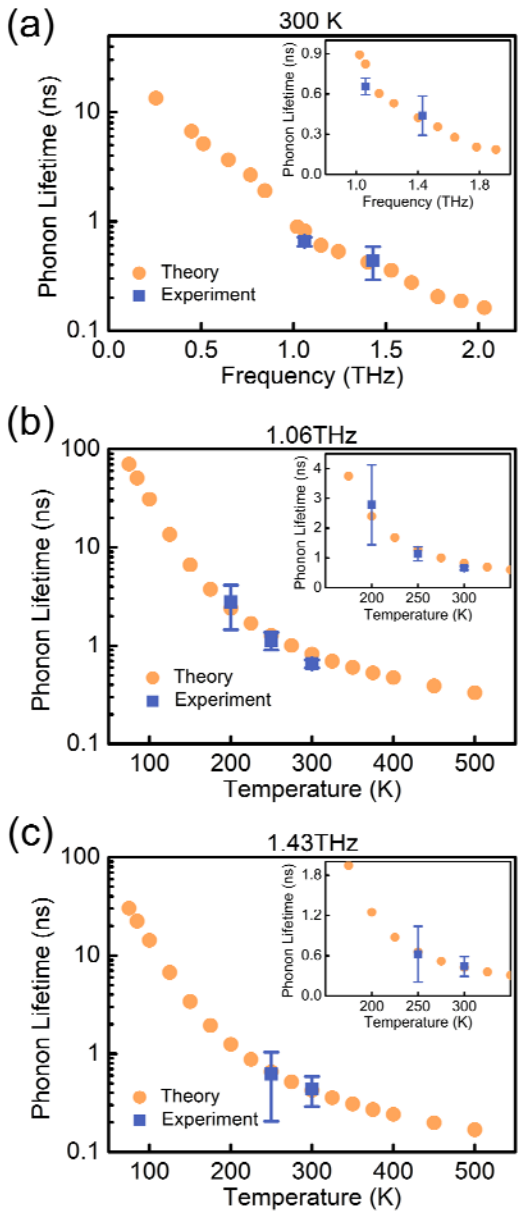

FIG. 6 (a) Calculated intrinsic phonon lifetimes (orange circles) of c-axis LA phonons in GaN at 300 K versus phonon frequency compared with measured data (blue squares). (b), (c) Calculated intrinsic phonon lifetimes at 1.06 and 1.43 THz versus temperature compared with measured data. The insets show the same data using a linear scale. The details of error bar calculations are given in Supplemental Material [32].

We performed first-principles calculations of three-phonon interactions to obtain intrinsic lifetimes of THz LA phonons propagating along the *c*-axis of GaN. Harmonic and anharmonic interatomic force constants were determined from density functional theory [36]

and density functional perturbation theory [37], respectively. The calculated lifetimes were given by the inverse of the total scattering rate which sums over all intrinsic scattering probabilities. The three-phonon scattering probabilities were obtained by using Eq. (2) in Ref. [12]. This calculation method is the same as that previously published in Ref. [26]. Figures 6(a), 6(b), and 6(c) show the calculated lifetimes compared with experimental results and indicate good agreement for both frequency and temperature dependences. Note that the calculated lifetimes at 80 K are much longer than those at 200 and 300 K (nearly 25 and 75 times greater, respectively), thus justifying Eq. (3). The measurements provide a direct test of *ab initio* calculations of anharmonic phonon-phonon interactions. We separately calculated scattering by isotope disorder in natural GaN and found that it is entirely negligible in the frequency range 1–1.4 THz. In the temperature and frequency ranges considered here, four-phonon scattering is expected to also be negligible. A recent study comparing thermal conductivity measurements with *ab initio* calculations suggested that four-phonon scattering may be important in GaN, particularly at temperature range 300–850 K [38]. However, for the frequency range (1–1.4 THz) considered here, four-phonon scattering was shown to be orders of magnitude weaker than three-phonon scattering in BAs, Si, and diamond, even at a higher temperature of 1000 K [39].

TABLE I. Contributions of different three-phonon processes to the total scattering rate for 1.06 THz LA phonons along the c-axis in isotopically pure GaN at 300 K and 50 K. L, T, A, and O represent longitudinal, transverse, acoustic, and optical, respectively. O may include some high-frequency acoustic modes due to branch crossings. Several processes (such as LA+LA→TA, LA+LA→LA) are not listed in the table because their contributions are negligible or not allowed by conservation conditions.

Scattering Process	**Total rate at 300 K**	**Total rate at 50 K**
LA+TA→TA	0.14%	0.89%
LA→TA+TA	0.10%	3.78%
LA→LA+TA	0.02%	0.74%
LA+TA→LA	4.96%	84.30%
LA+TA→O	1.60%	6.05%
LA+LA→O	0.48%	1.90%
LA+O→O	92.70%	2.34%

To get insight into the underlying physics, we examined the scattering processes that limit the 1.06 THz LA phonon lifetimes at 300 and 50 K (see Table I) and calculated the phonon density of states in GaN weighted by the Bose-Einstein distribution at different temperatures (see Fig. 7). We categorize three-phonon processes into three groups: AAA, AAO, and AOO, depending on the nature of the phonons involved, acoustic (A) or optical (O). Surprisingly, we found that AOO processes are the dominant scattering channel for 1 THz LA phonons at RT. In particular, interactions of 1 THz LA phonons and the six highest frequency optical branches (above 15 THz, i.e., above the frequency gap shown in Fig. 7) account for 90% of the overall scattering rate. Three-phonon interactions (lowest order intrinsic scattering in the perturbation theory) conserve energy and crystal momentum. For the low THz phonon frequency, small wavevector LA phonons considered here, this requires that the frequency difference between the two other phonons involved in scattering

interactions must also be identically small (~1 THz). The six highest frequency optic branches are less dispersive than the other branches and have many modes packed closely together with relatively small frequency differences (see Fig. 1 of Ref. [12]). Thus, scattering interactions involving low frequency LA phonons with two high frequency optic modes are not strongly limited by energy conservation and this channel is relatively important. Similar scattering has been observed and discussed for Pb-based rocksalt [40] and Li-based antifluorite chalcogenides [41].

Although optical phonons contribute little to thermal energy transfer because of their low group velocities, our results imply that optical phonons provide strong scattering channels for THz acoustic phonons at RT. In contrast, three-phonon scattering at 50 K is dominated by different kinds of AAA processes, accounting for ~90% of the total scattering rate, due to depopulation of high-frequency optical branches at low temperatures as illustrated in Fig. 7. This effect also results in the very steep low-temperature dependence (<150 K) of the calculated phonon lifetimes shown in Figs. 6(b) and 6(c). In previous studies of sub-THz coherent phonons, the discussion of the acoustic phonon lifetime was limited to AAA scattering processes [21-23,25]. Our results indicate that while this approach is perfectly reasonable for analyzing measurements at 50 K [22], the AOO process is an important scattering channel at RT for low THz frequencies.

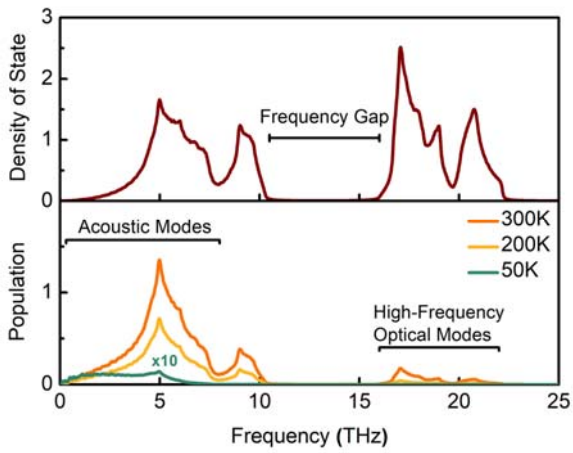

FIG. 7 Phonon density of states in GaN (brown curve). Phonon populations versus frequency at 300 K (orange curve), 200 K (yellow curve), and 50 K (green curve) are determined by the density of states weighted by the Bose-Einstein distribution.

Our measurements indicate that intrinsic lifetimes of 1–1.4 THz LA phonons in GaN (438.3–655 ps) are shorter than the calculated LA phonon lifetimes in Si (~1.6 ns at 1 THz [2]), even though GaN has higher thermal conductivity than Si (~150 $Wm^{-1}K^{-1}$ at RT). This means that the relative contribution of low-THz phonons to thermal transport is significantly smaller for GaN. Indeed, we can estimate the contribution of LA phonons at frequencies below 1.43 THz directly from the experimental data: extrapolating the frequency dependence of the phonon lifetime down to zero frequency using a power law, and employing the relaxation time approximation, which works reasonably well for GaN at RT [42]. We get

$$k_{LA}(\omega < \omega_0) = \frac{1}{3}\int_0^{\omega_0} C_\omega v_L^2 \, \tau_\omega \mathrm{d}\omega \tag{4}$$

where C_ω is volumetric specific heat per unit frequency interval, $v_L = 8020\, m/s$ is the longitudinal acoustic velocity and τ_ω is the phonon lifetime. In the low-frequency limit

($\hbar\omega \ll k_B T$), volumetric specific heat can be expressed as $C_\omega = \frac{k_B \omega^2}{2\pi^2 v_L^3}$. The frequency dependence of the phonon lifetime is assumed to follow a power law $\tau_\omega = \frac{a}{\omega^\alpha}$, where a is a constant and $\alpha = 1.34$ is obtained from the experimental data (655 and 438.3 ps for 1.06 and 1.43 THz). Thus, we get

$$k_{LA}(\omega < \omega_0) = \frac{k_B a}{6\pi^2 v_L} \int_0^{\omega_0} \omega^{2-\alpha}\, d\omega = \frac{k_B \tau_0 \omega_0^3}{6\pi^2 v_L (3-\alpha)} \quad (5).$$

Replacing $\omega = 2\pi f$, we get

$$k_{LA}(f < f_0) = \frac{4\pi k_B \tau_0 f_0^3}{3 v_L (3-\alpha)} \approx 5.6\ \mathrm{W/mK} \quad (6)$$

where f_0=1.43 THz, τ_0=438.3 ps, and k_B is the Boltzmann constant. This estimate does not account for TA branches, but even assuming that their contribution is twice as much, the total contribution of phonons below 1.43 THz to the thermal conductivity of natural GaN will be just $5.6 \times 3/230 \approx 7\%$. It agrees with a recent numerical study [42] which reported that the contribution of phonons below 2 THz is ~10%. On the other hand, a large contribution to thermal conductivity of GaN (60% for the isotopically pure material) is predicted to come from a narrow band of high-frequency acoustic phonons between 5–7 THz [42]. The small contribution of low-THz, long-MFP phonons means that we can expect a much smaller size effect for thermal transport in GaN at the micron scale compared to Si, which is consistent with the calculated thermal conductivity accumulation vs phonon MFP [42]. This implies that the heat dissipation performance of GaN in nanoelectronics will not be degraded as much by finite size effects as in the case of Si. Similar behavior can be expected to occur in other high

k materials with large frequency gap such as BAs [13], BSb [13], BeSe [43], and GeC [43].

IV. CONCULSION

We have reported the measurements of intrinsic lifetimes and MFPs of long-lived THz LA phonons in GaN at RT. The measurements are in good agreement with *ab initio* three-phonon scattering calculations which indicate that high-frequency optical modes provide the dominant scattering channel for the LA phonon decay. Our results indicate that in contrast to Si, low-THz phonons contribute little to thermal conductivity of GaN, which implies better performance of GaN as a heat dissipation material at the microscale. We note that the measured lifetimes correspond to linewidths below 10^{-2} meV, which is far beyond the resolution limitations of inelastic x-ray and neutron scattering techniques (in addition, the required wavevector resolution would be ~10^{-4} nm^{-1}, which is even less realistic) [14,15]. Thus laser-generation of coherent phonons offers a unique way to measure lifetimes and MFPs of long-lived THz acoustic phonons in high thermal conductivity materials.

ACKNOWLEDGEMENTS

The contribution by T.-H.C. and C.-K.S. was supported by the Ministry of Science and Technology, Taiwan through MOST 106-2112-M-002-004-MY3. First-principles calculations were supported by the U. S. Department of Energy, Office of Science, Basic Energy Sciences, Materials Sciences and Engineering Division. The contribution by A.A.M. and K.A.N. was supported by the U.S. Department of Energy, Office of Basic Energy Sciences under Award No. DE-FG02-00ER15087. The contribution by J.S.G., D.W.S., R.L.F., and A.B. was supported by the University of Houston Grants to Enhance Research Program (Grant #55322).

REFERENCE

[1] I. Maasilta and A. J. Minnich, Physics Today **67**, 27 (2014).

[2] A. Ward and D. A. Broido, Physical Review B **81**, 085205 (2010).

[3] J. A. Johnson, A. A. Maznev, J. Cuffe, J. K. Eliason, A. J. Minnich, T. Kehoe, C. M. S. Torres, G. Chen, and K. A. Nelson, Physical Review Letters **110**, 025901 (2013).

[4] Y. Hu, L. Zeng, A. J. Minnich, M. S. Dresselhaus, and G. Chen, Nat Nanotechnol **10**, 701 (2015).

[5] J. A. Johnson, J. K. Eliason, A. A. Maznev, T. Luo, and K. A. Nelson, Journal of Applied Physics **118**, 155104 (2015).

[6] R. B. Wilson and D. G. Cahill, Applied Physics Letters **107**, 203112 (2015).

[7] D. G. Cahill, P. V. Braun, G. Chen, D. R. Clarke, S. Fan, K. E. Goodson, P. Keblinski, W. P. King, G. D. Mahan, A. Majumdar *et al.*, Applied Physics Reviews **1**, 011305 (2014).

[8] J. Cuffe, J. K. Eliason, A. A. Maznev, K. C. Collins, J. A. Johnson, A. Shchepetov, M. Prunnila, J. Ahopelto, C. M. Sotomayor Torres, G. Chen *et al.*, Physical Review B **91**, 245423 (2015).

[9] L. Zeng, K. C. Collins, Y. Hu, M. N. Luckyanova, A. A. Maznev, S. Huberman, V. Chiloyan, J. Zhou, X. Huang, K. A. Nelson *et al.*, Sci Rep **5**, 17131 (2015).

[10] D. A. Broido, M. Malorny, G. Birner, N. Mingo, and D. A. Stewart, Applied Physics Letters

91, 231922 (2007).
[11] L. Lindsay, D. A. Broido, and T. L. Reinecke, Physical Review B **87**, 165201 (2013).
[12] L. Lindsay, D. A. Broido, and T. L. Reinecke, Physical Review Letters **109**, 095901 (2012).
[13] L. Lindsay, D. A. Broido, and T. L. Reinecke, Physical Review Letters **111**, 025901 (2013).
[14] O. Delaire, J. Ma, K. Marty, A. F. May, M. A. McGuire, M. H. Du, D. J. Singh, A. Podlesnyak, G. Ehlers, M. D. Lumsden *et al.*, Nat Mater **10**, 614 (2011).
[15] J. Ma, O. Delaire, E. D. Specht, A. F. May, O. Gourdon, J. D. Budai, M. A. McGuire, T. Hong, D. L. Abernathy, G. Ehlers *et al.*, Physical Review B **90**, 134303 (2014).
[16] J. W. L. Pang, W. J. L. Buyers, A. Chernatynskiy, M. D. Lumsden, B. C. Larson, and S. R. Phillpot, Physical Review Letters **110**, 157401 (2013).
[17] P. F. Lory, S. Pailhes, V. M. Giordano, H. Euchner, H. D. Nguyen, R. Ramlau, H. Borrmann, M. Schmidt, M. Baitinger, M. Ikeda *et al.*, Nat Commun **8**, 491 (2017).
[18] Z. Tian, M. Li, Z. Ren, H. Ma, A. Alatas, S. D. Wilson, and J. Li, J Phys Condens Matter **27**, 375403 (2015).
[19] Z. Tian, J. Garg, K. Esfarjani, T. Shiga, J. Shiomi, and G. Chen, Physical Review B **85**, 184303 (2012).
[20] B. C. Daly, K. Kang, Y. Wang, and D. G. Cahill, Physical Review B **80**, 174112 (2009).
[21] J. Cuffe, O. Ristow, E. Chávez, A. Shchepetov, P. O. Chapuis, F. Alzina, M. Hettich, M. Prunnila, J. Ahopelto, T. Dekorsy *et al.*, Physical Review Letters **110**, 095503 (2013).
[22] R. Legrand, A. Huynh, B. Jusserand, B. Perrin, and A. Lemaître, Physical Review B **93**, 184304 (2016).
[23] T.-M. Liu, S.-Z. Sun, C.-F. Chang, C.-C. Pan, G.-T. Chen, J.-I. Chyi, V. Gusev, and C.-K. Sun, Applied Physics Letters **90**, 041902 (2007).
[24] P.-A. Mante, Y.-R. Huang, S.-C. Yang, T.-M. Liu, A. A. Maznev, J.-K. Sheu, and C.-K. Sun, Ultrasonics **56**, 52 (2015).
[25] F. J. Wei, Y. H. Yeh, J. K. Sheu, and K. H. Lin, Sci Rep **6**, 28577 (2016).
[26] A. A. Maznev, T. C. Hung, Y. T. Yao, T. H. Chou, J. S. Gandhi, L. Lindsay, H. D. Shin, D. W. Stokes, R. L. Forrest, A. Bensaoula *et al.*, Applied Physics Letters **112**, 061903 (2018).
[27] A. A. Maznev, K. J. Manke, K.-H. Lin, K. A. Nelson, C.-K. Sun, and J.-I. Chyi, Ultrasonics **52**, 1 (2012).
[28] A. Huynh, B. Perrin, B. Jusserand, and A. Lemaître, Applied Physics Letters **99**, 191908 (2011).
[29] Y. Won, J. Cho, D. Agonafer, M. Asheghi, and K. E. Goodson, IEEE Transactions on Components, Packaging and Manufacturing Technology **5**, 737 (2015).
[30] C. Mion, J. F. Muth, E. A. Preble, and D. Hanser, Applied Physics Letters **89**, 092123 (2006).
[31] C.-K. Sun, J.-C. Liang, and X.-Y. Yu, Physical Review Letters **84**, 179 (2000).
[32] See Supplemental Material at [URL] for details on (A) sample fabrication and

characterization, (B) experimental setups of optical pump probe spectroscopy and optical microscope, (C) power-dependent measurements, and (D) error calculations of acoustic attenuation (P3/P1) and intrinsic phonon lifetime.

[33] G.-W. Chern, K.-H. Lin, and C.-K. Sun, Journal of Applied Physics **95**, 1114 (2004).

[34] K.-H. Lin, G.-W. Chern, Y.-K. Huang, and C.-K. Sun, Physical Review B **70**, 073307 (2004).

[35] S. Wu, P. Geiser, J. Jun, J. Karpinski, and R. Sobolewski, Physical Review B **76**, 085210 (2007).

[36] W. Kohn and L. J. Sham, Physical Review **140**, A1133 (1965).

[37] S. Baroni, S. de Gironcoli, A. Dal Corso, and P. Giannozzi, Reviews of Modern Physics **73**, 515 (2001).

[38] Q. Zheng, C. Li, A. Rai, J. H. Leach, D. A. Broido, and D. G. Cahill, Physical Review Materials **3**, 014601 (2019).

[39] T. Feng, L. Lindsay, and X. Ruan, Physical Review B **96**, 161201(R) (2017).

[40] S. Lee, K. Esfarjani, T. Luo, J. Zhou, Z. Tian, and G. Chen, Nature Communications **5**, 3525 (2014).

[41] S. Mukhopadhyay, L. Lindsay, and D. S. Parker, Physical Review B **93**, 224301 (2016).

[42] J. Garg, T. Luo, and G. Chen, Applied Physics Letters **112**, 252101 (2018).

[43] L. Lindsay, D. A. Broido, and T. L. Reinecke, Physical Review B **88**, 144306 (2013).